Iranian Journal of Numerical Analysis and Optimization
Vol. 16, No. 1, 2026, pp 38–60
https://doi.org/10.22067/ijnao.2025.93661.1654
https://ijnao.um.ac.ir/

Research Article

Numerical exploration of pollutant transport using stochastic fractional diffusion and Karhunen–Loève expansion

Z. Moniri, A. Babaei*, and B. Parsa Moghaddam

Abstract

This study explores a fractional time-space stochastic diffusion equation for modeling pollutant concentration, incorporating Caputo fractional derivatives and fractional Laplacians to capture anomalous diffusion. Stochastic noise, modeled via Brownian motion and Brownian bridges, is simulated using the Karhunen–Loève expansion (KLE). The equation's formulation, along with initial and boundary conditions, is presented. Analytical and numerical methods are discussed, emphasizing a hybrid framework combining fast Fourier transform, L1-algorithm, and KLE techniques. Numerical examples with sinc and Gaussian initial conditions highlight

*Corresponding author

Received 23 May 2025; revised 6 September 2025; accepted 27 September 2025

Zahra Moniri
Department of Applied Mathematics, University of Mazandaran, Babolsar, Iran. e-mail: z.moniri05@stu.umz.ac.ir

Afshin Babaei
Department of Applied Mathematics, University of Mazandaran, Babolsar, Iran. e-mail: babaei@umz.ac.ir

Behrouz Parsa Moghaddam
Department of Mathematics, La.C., Islamic Azad University, Lahijan, Iran. e-mail: bparsa@fe.up.pt

This article was suggested by the scientific committee of the 17th seminar on differential equation and dynamical system for publication in IJNAO, which was accepted after independent review.

How to cite this article
Moniri, Z., Babaei, A. and Parsa Moghaddam, B., Numerical exploration of pollutant transport using stochastic fractional diffusion and Karhunen–Loève expansion. *Iran. J. Numer. Anal. Optim.*, 2026; 16(1): 38-60. https://doi.org/10.22067/ijnao.2025.93661.1654

the superior accuracy and efficiency of the KLE approach over traditional Euler methods, revealing the significant influence of fractional parameters on pollutant dispersion dynamics and their potential for environmental modeling applications.

AMS subject classifications (2020): 35R60, 60G22, 65M75, 60H30, 76R50, 86A05

Keywords: Noninteger order probabilistic transport equation; Memory-dependent time derivatives; Eigenfunction decomposition methods; Contaminant transport simulation; Numerical approximation strategies.

1 Introduction

Fractional stochastic diffusion equations (FSDEs) have become essential in modeling intricate phenomena across physical, biological, and engineering domains. By extending classical diffusion models through fractional derivatives, these equations effectively describe anomalous diffusion, where particle spread deviates from standard patterns [9, 3]. The inclusion of stochastic components further enhances their capability to represent inherent randomness in various systems, such as fluid dynamics in porous media and particle movement in disordered structures [28, 30].

These equations play a crucial role in diverse applications. In ecology and biology, they model species dispersion and organism movement in heterogeneous environments, providing insights into ecosystem dynamics [3, 15]. Within engineering and physics, FSDEs describe heat, mass, and momentum transport in complex materials, as well as energy transfer in oscillator chains and particle behavior in nonequilibrium systems [13, 23]. Additionally, chemical engineering relies on FSDEs to analyze reaction-diffusion systems, helping predict chemical species' behavior in reactors and industrial processes [2, 10].

Addressing FSDEs requires sophisticated mathematical and computational techniques. Methods such as the tanh-coth approach, Caputo derivatives, and finite difference schemes provide both exact and approximate solutions [15, 1]. More advanced frameworks, including the Carathéodory approximation and the variational iteration method (VIM) combined with the Elzaki transform, enhance solution stability and convergence, ensuring their reliability in practical applications [28, 19].

Despite their broad applicability, FSDEs present significant computational challenges due to their complexity. Ongoing research focuses on refining numerical techniques and expanding their use in fields like finance and advanced materials science [25, 26]. Additionally, efforts are directed

toward developing generalized models that incorporate stochastic resetting and fractional Fokker-Planck equations, further broadening their scope [6, 24].

Recent comprehensive reviews have systematically examined the rapid evolution of numerical methods for fractional stochastic partial differential equations, highlighting significant advances in spectral methods, finite element approaches, and their practical implementations across various disciplines [17]. Contemporary developments have extended these methodologies to multi-dimensional frameworks, establishing robust computational strategies that combine L1-algorithms with FFT-based approaches for handling complex spatio-temporal noise structures [18].

In this research, we investigate a fractional time-space stochastic diffusion equation (FTSSDE) designed to model the concentration of pollutants in a given medium. The governing equation is expressed as

$$ {}^{c}\partial_t^{\alpha} C(x,t) + \kappa_\beta(-\Delta)^{\beta/2} C(x,t) = \sigma\eta(x,t), \quad 0 < \alpha \leq 1, \quad 0 < \beta \leq 2, \tag{1} $$

where the spatial domain is $x \in [c, c+L]$, time $t > 0$, and $C(x,t)$ represents the pollutant concentration. The equation incorporates fractional derivatives in both time and space, capturing anomalous diffusion processes influenced by stochastic noise. The initial condition is specified as

$$ C(x,0) = C_0(x), \quad x \in [c, c+L], \tag{2} $$

indicating the initial distribution of the pollutant. The boundary condition is periodic, given by

$$ C(c,t) = C(c+L,t), \tag{3} $$

ensuring continuity of the concentration across the boundaries of the spatial domain.

The parameter κ_β governs the diffusivity, determining the rate at which the pollutant disperses through the medium. The fractional exponent β characterizes the type of diffusion: smaller values of β (closer to 0) correspond to super-diffusive behavior, where particles spread faster than in classical diffusion, while values approaching 2 indicate sub-diffusive behavior, where spreading is slower. The fractional time derivative, parameterized by α, introduces memory effects, allowing the model to account for historical states of the system. This framework is particularly useful for analyzing complex pollutant dynamics influenced by fractional and stochastic effects, such as those observed in heterogeneous or porous media.

The Caputo fractional time derivative ${}^{c}\partial_t^{\alpha} C(x,t)$ is defined for $0 < \alpha < 1$ as

$$ {}^{c}\partial_t^{\alpha} C(x,t) = \frac{1}{\Gamma(1-\alpha)} \int_0^t \frac{\partial C(x,\tau)}{\partial \tau} \frac{1}{(t-\tau)^{\alpha}}\, d\tau, \tag{4} $$

where Γ is the Gamma function, and the derivative accounts for nonlocal temporal effects. The spatial fractional Laplacian $(-\Delta)^{\beta/2} C(x,t)$, which governs the anomalous spatial diffusion, is defined in the one-dimensional case for $0 < \beta < 2$ as

$$ (-\Delta)^{\beta/2} C(x,t) = -\frac{1}{2\cos(\pi\beta/2)} \left({}_{c}D_x^{\beta} C(x,t) + {}_{x}D_{c+L}^{\beta} C(x,t) \right), \tag{5} $$

where ${}_{c}D_x^{\beta} C(x,t)$ and ${}_{x}D_{c+L}^{\beta} C(x,t)$ are the left and right Riemann–Liouville fractional derivatives of order β, respectively. Let $n = \lceil \beta \rceil$, the smallest integer greater than or equal to β. These derivatives are given by

$$ {}_{c}D_x^{\beta} C(x,t) = \frac{1}{\Gamma(n-\beta)} \frac{d^n}{dx^n} \int_c^x (x-\xi)^{n-\beta-1} C(\xi,t)\, d\xi, \tag{6} $$

$$ {}_{x}D_{c+L}^{\beta} C(x,t) = \frac{(-1)^n}{\Gamma(n-\beta)} \frac{d^n}{dx^n} \int_x^{c+L} (\xi-x)^{n-\beta-1} C(\xi,t)\, d\xi. \tag{7} $$

These expressions capture the nonlocal spatial interactions, allowing the model to describe long-range dependencies in the pollutant's spread. The stochastic term $\eta(x,t) = W(x)\mathbb{B}_{\text{Bridge}}(t)$ introduces randomness into the system, where $W(x)$ represents a Brownian motion in the spatial coordinate, modeling random fluctuations in the pollutant source, and $\mathbb{B}_{\text{Bridge}}(t)$ is a Brownian bridge in time, ensuring that the noise is constrained to specific temporal behavior (e.g., returning to a reference state at the boundaries of the time interval).

This model extends traditional diffusion equations by incorporating fractional calculus and stochastic processes, making it suitable for scenarios where classical diffusion models fail, such as in turbulent flows, fractured aquifers, or atmospheric pollutant dispersion. The combination of fractional derivatives and stochastic noise enables the model to capture both memory effects and random environmental influences, providing a robust framework for studying complex transport phenomena. Potential applications include environmental engineering, where understanding pollutant dispersion is critical for designing mitigation strategies, and in hydrology, for modeling contaminant transport in groundwater systems. Future work could explore numerical methods for solving the FTSSDE or extend the model to higher dimensions for more realistic representations of physical systems.

Pollutant dispersion in natural environments often exhibits anomalous diffusion characteristics due to the complexity of the medium, such as soil heterogeneity, turbulent atmospheric layers, and porous geological formations. Classical diffusion models assume a Gaussian spread of pollutants, which fails to capture real-world scenarios where pollutants experience long-range

correlations, memory effects, and heterogeneous transport mechanisms. The FTSSDE provides a more generalized framework, incorporating both temporal and spatial fractional derivatives to model nonlocal effects and power-law decay, leading to a more accurate representation of pollutant concentration in diverse environmental settings [7, 11, 27].

Recent advances in atmospheric science have demonstrated the effectiveness of fractional stochastic advection-diffusion frameworks for modeling moisture transport at ocean-atmosphere interfaces, where temporal memory effects and nonlocal turbulent diffusion mechanisms play crucial roles in boundary layer dynamics [16]. These developments underscore the growing recognition that fractional stochastic models provide superior accuracy in capturing environmental transport phenomena compared to classical approaches.

Environmental factors such as fluctuating wind patterns, temperature variations, and chemical reactions introduce inherent randomness into pollutant transport. Traditional deterministic models cannot adequately account for such uncertainties, making stochastic modeling essential. FTSSDEs integrate stochastic noise to reflect the probabilistic nature of diffusion, ensuring realistic predictions of pollutant spread under varying conditions. This stochastic component enables the model to describe the erratic dispersion of pollutants in urban air pollution, riverine contamination, and subsurface transport, where external influences create unpredictable deviations in concentration levels [29, 31].

The incorporation of stochastic components in pollutant transport modeling is not merely a mathematical abstraction but reflects fundamental physical realities that govern environmental systems. Environmental variability introduces inherent randomness through fluctuating meteorological conditions, such as turbulent wind patterns, temperature gradients, and precipitation variability, which directly affect dispersion rates and directions. Additionally, subsurface heterogeneity creates random spatial variations in hydraulic conductivity, porosity, and chemical reaction rates that cannot be deterministically characterized at practical scales. Model uncertainty arises from incomplete knowledge of initial pollutant distributions, boundary conditions, and measurement noise in monitoring systems. Furthermore, multi-scale interactions between molecular diffusion, advective transport, and chemical transformations exhibit stochastic behavior due to the complex interplay between microscopic and macroscopic processes. From a regulatory perspective, probabilistic risk assessment requires stochastic modeling to quantify uncertainty bounds and confidence intervals, enabling robust environmental management decisions under uncertainty. Traditional deterministic models fail to capture these random fluctuations, potentially leading to significant underestimation or overestimation of pollutant concentrations, which can have serious implications for public health risk assessment and environmental remediation strategies.

In addition to stochasticity and anomalous diffusion, pollutant transport often occurs in highly heterogeneous media where physical and chemical properties vary significantly over space and time. FTSSDEs allow for flexible adaptation to these conditions by tuning the order of fractional derivatives, effectively capturing the influence of porous structures, adsorption-desorption dynamics, and multi-phase flow interactions. This adaptability makes FTSSDEs particularly valuable for predicting long-term pollutant behavior in groundwater contamination, atmospheric dispersion modeling, and large-scale ecological impact assessments. The development of robust numerical and analytical methods further enhances their applicability, making FTSSDEs a powerful tool for environmental scientists and engineers [12, 14].

To address the computational challenges posed by FTSSDEs, we develop a hybrid numerical framework that combines three sophisticated techniques: (1) Fast Fourier transform (FFT) implementation for efficient spatial discretization of fractional Laplacians, exploiting the spectral properties of these operators in frequency domain; (2) L1-algorithm for robust temporal approximation of Caputo fractional derivatives, providing first-order accuracy with optimal computational complexity; and (3) Karhunen–Loève expansion (KLE) for accurate simulation of stochastic noise components, offering superior convergence properties compared to traditional Euler-Maruyama schemes. This integrated approach enables us to achieve computational efficiency while maintaining high numerical accuracy for complex fractional stochastic systems.

The primary contributions of this work include: (i) demonstrating that KLE-based noise simulation achieves mean squared errors (MSEs) approximately three orders of magnitude lower than conventional Euler methods; (ii) establishing superior convergence rates for the KLE approach (orders 1.57–5.43) compared to Euler schemes (orders 1.19–2.73); (iii) proving computational efficiency gains where KLE with 128 grid points outperforms Euler with 512 points; and (iv) providing a comprehensive analysis of fractional parameter effects on pollutant dispersion dynamics in stochastic environments.

The remainder of this article is organized as follows. Section 2 provides the preliminary concepts, including definitions of Brownian motion, Brownian bridge, and the KLE, which form the foundation of our stochastic modeling approach. Section 3 details the KLE simulation of Brownian sheet noise, supported by visualizations of the stochastic process. Section 4 presents the implementation of the FFT for solving the FTSSDE, alongside the L1-algorithm for approximating the Caputo fractional derivative. Section 5 discusses the numerical implementation, including computational details and illustrative examples with sinc initial conditions. Finally, Section 6 concludes the study, summarizing key findings and outlining potential applications and future research directions in environmental modeling.

2 Preliminaries

Modeling pollutant dispersion in the environment requires mathematical frameworks that effectively capture randomness, nonstationarity, and spatial-temporal correlations. Brownian motion, Brownian bridge, and the KLE provide significant advantages in this regard. Brownian motion (Definition 1) serves as a fundamental stochastic model for the random diffusion of pollutants in fluids, with extensions such as fractional Brownian motion allowing for greater flexibility in modeling persistence and roughness [14, 22]. The Brownian bridge (Definition 2), a constrained variant of Brownian motion, is particularly useful when pollutant concentrations are known at specific times or locations, ensuring consistency with boundary conditions and enhancing statistical inferences [14, 5].

Definition 1 (Brownian motion [14])**.** A stochastic process $\{W(t)\}_{t\geq 0}$ is termed a Brownian motion if it constitutes a real-valued Gaussian process satisfying the following conditions:

i) Its sample paths are continuous functions of t;

ii) It possesses a zero mean function, that is, $\mathbb{E}[W(t)] = 0$ for all $t \geq 0$;

iii) Its covariance structure is characterized by $\mathrm{Cov}(W(s), W(t)) = \min(s, t)$ for all $s, t \geq 0$.

Definition 2 (Brownian Bridge [14])**.** A stochastic process $\{\mathbb{B}_{\mathrm{Bridge}}(t)\}_{t\in[0,T_f]}$ is termed a Brownian bridge if it constitutes a Gaussian process with the following properties:

i) It satisfies the boundary constraints $\mathbb{B}_{\mathrm{Bridge}}(0) = \mathbb{B}_{\mathrm{Bridge}}(T_f) = 0$ almost surely;

ii) It has a zero mean function, that is, $\mathbb{E}[\mathbb{B}_{\mathrm{Bridge}}(t)] = 0$ for all $t \in [0, T_f]$;

iii) Its covariance structure is characterized by $\mathrm{Cov}(\mathbb{B}_{\mathrm{Bridge}}(s), \mathbb{B}_{\mathrm{Bridge}}(t)) = \min(s, t) - st$ for all $s, t \in [0, T_f]$.

3 Karhunen–Loève expansion

The KLE is a powerful technique for reducing the dimensionality of stochastic processes, extracting dominant stochastic components from observed data to construct efficient empirical models. By providing accurate and computationally efficient representations of complex environmental processes, KLE plays a crucial role in stochastic simulations and predictive modeling [4, 20, 21]. These methods collectively improve the precision, adaptability, and computational feasibility of pollutant modeling, enabling more robust analysis and prediction of environmental phenomena.

For a stochastic process $U(x,\omega)$ defined on the spatial domain $x \in \mathcal{R}$, the KLE provides a representation using orthogonal functions and uncorrelated random variables.

If we denote the mean function as $\mu(x) = \mathbb{E}[U(x,\omega)]$, we can focus on the centered process $U(x,\omega) - \mu(x)$. Our goal is to represent the sample paths of this centered process as a series expansion using an orthonormal basis $\{\phi_n : n \in \mathbb{N}\}$ of $L^2(\mathcal{R})$:

$$U(x,\omega) - \mu(x) = \sum_{n=1}^{\infty} \sqrt{\lambda_n}\phi_n(x)\xi_n(\omega). \tag{8}$$

The random coefficients $\xi_n(\omega)$ in this expansion are given by

$$\xi_n(\omega) := \frac{1}{\sqrt{\lambda_n}} \langle U(x,\omega) - \mu(x), \phi_n(x) \rangle_{L^2(\mathcal{R})}. \tag{9}$$

Let us denote the covariance function of $U(x,\omega)$ as $\mathrm{Cov}(x,y)$. We can then define an integral operator $\mathcal{C}$ by

$$(\mathscr{C}\phi)(x) := \int_{\mathcal{R}} \mathcal{C}ov(x,y)\phi(y)\,dy, \quad \phi \in L^2(\mathcal{R}). \tag{10}$$

This framework allows us to decompose the stochastic process into deterministic spatial modes $\phi_n(x)$ and random coefficients $\xi_n(\omega)$.

The KLE is given by (8) when the functions ϕ_n are chosen as the eigenfunctions of the operator $\mathscr{C}[\cdot]$. This approach represents a stochastic process as an infinite series of orthogonal basis functions, each weighted by uncorrelated random variables. The values λ_n are the associated eigenvalues of the operator $\mathscr{C}[\cdot]$.

3.1 Karhunen–Loève simulation of Brownian sheet noise $W(x)\mathbb{B}_{\mathrm{Bridge}}(t)$

Brownian Sheet noise, denoted as $W(x)\mathbb{B}_{\mathrm{Bridge}}(t)$, is the product of a Wiener process $W(x)$ and a Brownian bridge $\mathbb{B}_{\mathrm{Bridge}}(t)$. To derive its KLE, we can combine the expansions of its components.

First, recall the KLE of the Brownian bridge $\mathbb{B}_{\mathrm{Bridge}}(t)$ on $T_f = [0,1]$:

$$\mathbb{B}_{\mathrm{Bridge}}(t) = \sum_{j=1}^{\infty} \sqrt{2}\frac{\sin(j\pi t)}{\pi j}\xi_j, \quad \xi_j \sim \mathcal{N}(0,1) \text{ iid}, \tag{11}$$

and the KLE of the Wiener process $W(x)$ on $x \in [0,1]$:

$$W(x) = \sum_{n=1}^{\infty} \frac{2\sqrt{2}\sin\left(\left(n-\frac{1}{2}\right)\pi x\right)}{(2n-1)\pi}\eta_n, \quad \eta_n \sim \mathcal{N}(0,1) \text{ iid.} \tag{12}$$

To obtain the KLE of Brownian sheet noise $W(x)\mathbb{B}_{\text{Bridge}}(t)$, we multiply these two expansions:

$$W(x)\mathbb{B}_{\text{Bridge}}(t) = \sum_{n=1}^{\infty}\sum_{j=1}^{\infty} \frac{4\sin\left(\left(n-\frac{1}{2}\right)\pi x\right)\sin(j\pi t)}{(2n-1)\pi^2 j}\xi_j\eta_n. \tag{13}$$

This double series represents the KLE of Brownian sheet noise $W(x)\mathbb{B}_{\text{Bridge}}(t)$. Note that η_n and ξ_j are independent standard normal random variables.

To approximate sample paths of Brownian sheet noise on $[0,1]\times[0,1]$, we can truncate both series:

$$W(x)\mathbb{B}_{\text{Bridge}}(t) \approx W^N(x)\mathbb{B}^J_{\text{Bridge}}(t) = \sum_{n=1}^{N}\sum_{j=1}^{J} \frac{4\sin\left(\left(n-\frac{1}{2}\right)\pi x\right)\sin(j\pi t)}{(2n-1)\pi^2 j}\xi_j\eta_n, \tag{14}$$

where N and J are the number of terms used in the truncation for the Wiener process and Brownian bridge, respectively.

This expansion allows for efficient simulation of Brownian sheet noise by generating the required number of standard normal random variables and computing the finite sum. The accuracy of the approximation improves as N and J increase.

The Brownian sheet $W(x)\mathbb{B}_{\text{Bridge}}(t)$ were examined using parameters of 2^8 for the Wiener process terms (N), Brownian bridge terms (J), and spatial and temporal points. These processes were analyzed over a unit square domain. KLE simulation was employed to visualize these processes, as depicted in Figure 1. A three-dimensional surface plot in Subfigure 1a illustrates the spatial variations of the Brownian sheet, while Subfigure 1b provides a two-dimensional contour plot, elucidating the distribution of these variations across the domain.

4 Fast Fourier transform implementation for FTSSDE

To implement the FFT for the FTSSDE described in (1), we adopt the following detailed procedure:

First, we compute the FFT of each term in (1) with respect to the spatial coordinate x. For the Caputo fractional time derivative ${}^c\partial_t^\alpha C(x,t)$, the FFT with respect to x is expressed as

$$\mathcal{F}_x[{}^c\partial_t^\alpha C(x,t)] = {}^c\,\partial_t^\alpha \hat{C}(k,t),$$

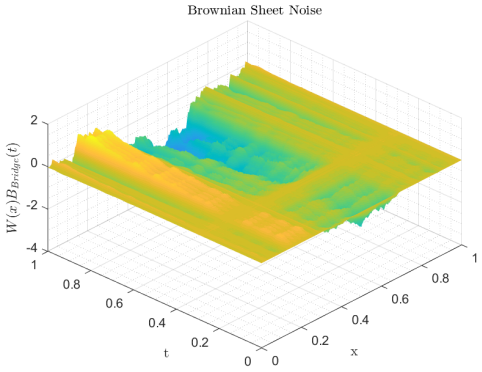

(a) Realization of the Brownian sheet $W(x)\mathbb{B}_{\text{Bridge}}(t)$ using KLE simulation.

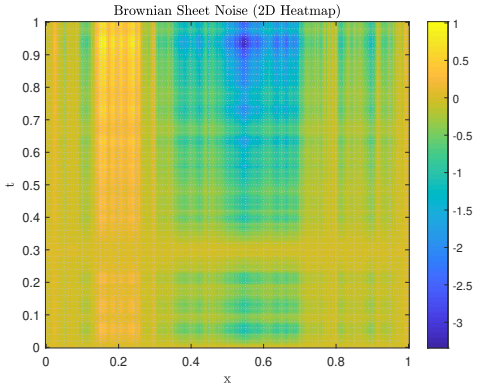

(b) Contour plot of the Brownian sheet $W(x)\mathbb{B}_{\text{Bridge}}(t)$ using KLE simulation.

Figure 1: Visual representations of the Brownian sheet generated via KLE simulation. (a) A 3D surface plot depicting the Brownian sheet. (b) A contour plot illustrating the Brownian sheet.

where $\hat{C}(k,t) = \mathcal{F}_x[C(x,t)]$ represents the Fourier transform of $C(x,t)$ in the spatial domain, and k denotes the wavenumber, which characterizes the spatial frequency.

For the fractional Laplacian term $(-\Delta)^{\beta/2}C(x,t)$, the FFT is given by

$$\mathcal{F}_x[(-\Delta)^{\beta/2}C(x,t)] = |k|^{\beta}\hat{C}(k,t),$$

where $|k|$ is the magnitude of the wavenumber, reflecting the scaling of the fractional Laplacian in the frequency domain.

Assuming the noise term $\eta(x,t)$ is spatially uncorrelated, its FFT is represented as $\hat{\eta}(k,t)$, preserving the stochastic properties in the frequency domain.

Applying the FFT with respect to x to both sides of (1), we obtain

$$\mathcal{F}_x\left[{}^c\partial_t^{\alpha}C(x,t)\right] = \mathcal{F}_x\left[-\kappa_{\beta}(-\Delta)^{\beta/2}C(x,t) + \sigma\eta(x,t)\right].$$

By substituting the Fourier transforms of the individual terms, the equation becomes

$${}^c\partial_t^{\alpha}\hat{C}(k,t) + \kappa_{\beta}|k|^{\beta}\hat{C}(k,t) = \sigma\hat{\eta}(k,t).$$

This transformed equation describes the dynamics of the system in the frequency-wavenumber domain, highlighting the interaction between the Caputo fractional time derivative and the spatial fractional Laplacian. The use of the one-dimensional FFT enables efficient computation of these spectral representations, significantly reducing the computational complexity for

large-scale or high-dimensional datasets. Recent computational advances have extended these FFT-based methodologies to two-dimensional fractional stochastic systems, demonstrating superior efficiency in handling spatio-temporal noise structures through hybrid L1-FFT approaches [18]. This integration of spectral methods with fractional calculus represents a significant advancement in numerical techniques for solving complex environmental transport equations. This approach not only facilitates numerical simulations but also provides deeper insights into the fractional and stochastic behaviors of the system, making it particularly suitable for applications involving anomalous diffusion or complex spatial structures.

4.1 Numerical approximation of the Caputo fractional derivative for $C(x,t)$

Consider a uniform partition of the time interval $[0, T_f]$ with time step Δt. The Caputo fractional derivative at time t_n is approximated using the L1-algorithm, as described in [8]. For a fractional order $0 \leq \alpha < 1$, the Caputo fractional derivative is defined as

$$ {}^{c}\partial_t^{\alpha} C(x,t_n) = \frac{1}{\Gamma(1-\alpha)} \int_{t_0}^{t_n} \frac{\partial C(x,\tau)}{\partial \tau} (t_n - \tau)^{-\alpha} d\tau. $$

This integral is discretized to yield the following approximation:

$$ {}^{c}\partial_t^{\alpha} C(x,t_n) \approx \frac{\Delta t^{-\alpha}}{\Gamma(2-\alpha)} \sum_{j=0}^{n-1} b_j^{(\alpha)} \left(C(x,t_{n-j}) - C(x,t_{n-j-1}) \right) + \mathcal{O}(\Delta t), \tag{15} $$

where the coefficients are given by $b_j^{(\alpha)} = (j+1)^{1-\alpha} - j^{1-\alpha}$.

This formulation enables an efficient and straightforward implementation of the L1-algorithm for approximating the Caputo fractional derivative of $C(x,t)$. By integrating this temporal discretization with spatial discretization techniques, such as the FFT for computing fractional Laplacians, we obtain a robust and computationally effective approach for solving FTSSDEs.

The flowchart in Figure 2 illustrates a comprehensive numerical algorithm for solving FTSSDEs that feature both temporal and spatial fractional operators. The algorithm begins with parameter initialization and proceeds through two parallel noise simulation approaches—the KLE for spectral accuracy and Euler-Maruyama for computational efficiency—before constructing the stochastic noise term. The core computational loop employs Fourier transforms to handle the fractional Laplacian operator in frequency space, implements the L1 algorithm for the time-

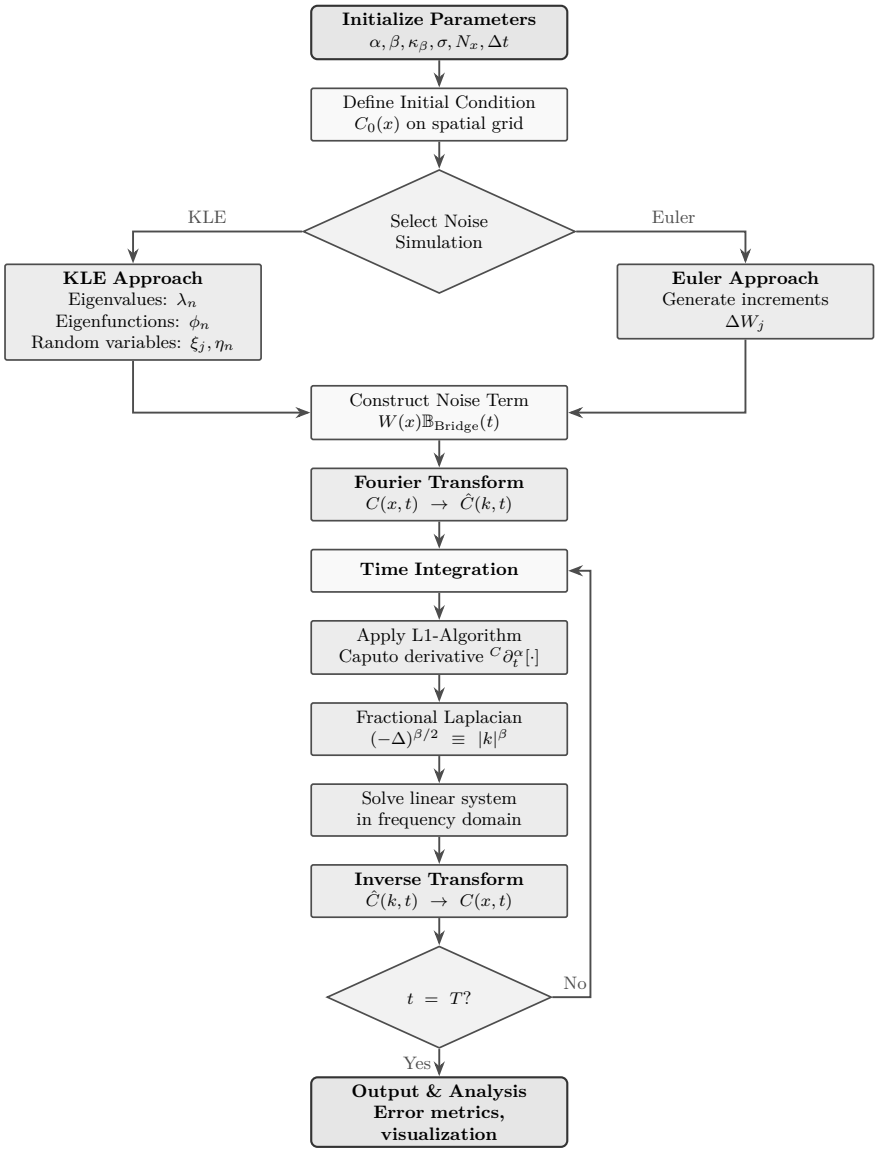

Figure 2: Numerical algorithm flowchart for solving the FTSSDEs with time-fractional Caputo derivative and space-fractional Laplacian operator. The algorithm employs Fourier spectral methods combined with either KLE or Euler-Maruyama discretization for stochastic noise simulation.

fractional Caputo derivative, and iteratively advances the solution until the final time is reached, making it suitable for modeling anomalous diffusion processes with memory effects and heavy-tailed spatial distributions.

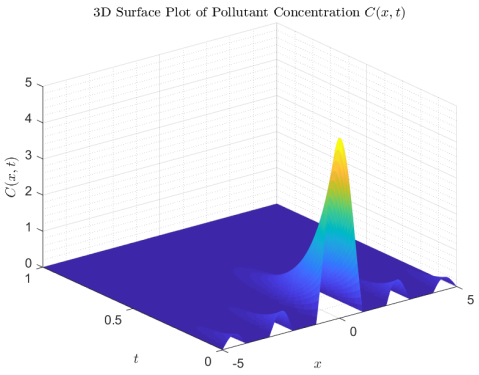

(a) Three-dimensional surface plot of pollutant concentration $C(x,t)$ using Euler Brownian noise simulation.

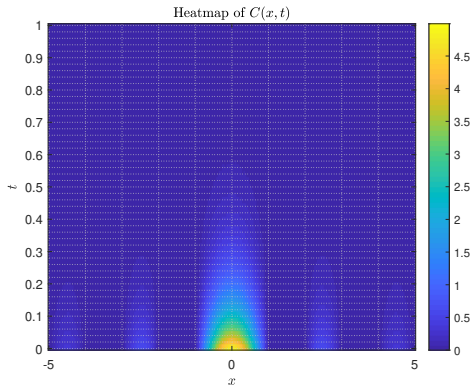

(b) Contour plot of pollutant concentration $C(x,t)$ with Euler simulation of Brownian noise.

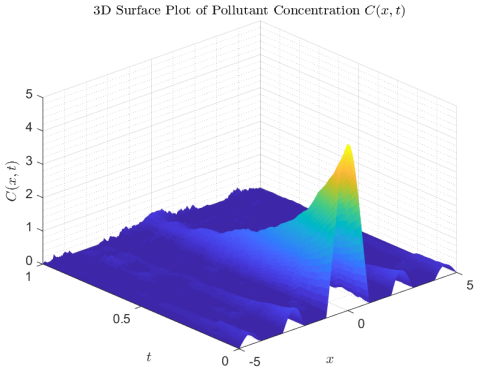

(c) Three-dimensional surface plot of pollutant concentration $C(x,t)$ using KLE Brownian noise simulation.

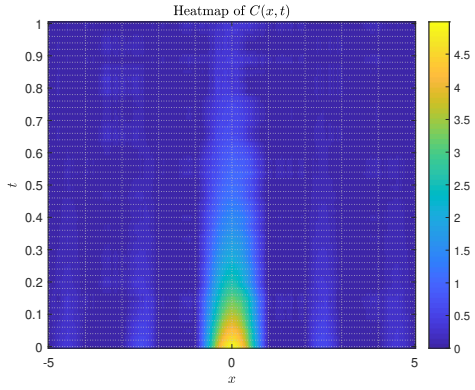

(d) Contour plot of pollutant concentration $C(x,t)$ with KLE Brownian noise simulation.

Figure 3: Example 1: Three-dimensional surface representations and contour plots displaying pollutant concentration $C(x,t)$ over space and time, using the sinc function as the initial condition.

5 Numerical implementation

To solve the FTSSDEs efficiently, we employed MATLAB's `fft` and `ifft` functions to handle the spatial discretization of partial differential equations via the FFT. This approach leverages the computational efficiency of FFT to approximate fractional Laplacians, significantly reducing the computational cost for large-scale simulations. To ensure the reproducibility of our results,

we initialized the random number generator with a fixed seed of 123 using MATLAB's Mersenne Twister algorithm. This configuration ensures consistent generation of pseudo-random numbers across multiple runs, allowing for reliable replication of results under identical conditions. By fixing the seed, we mitigate variability in stochastic simulations, which is critical for validating the robustness of our proposed scheme and for computing stable statistical metrics, such as confidence intervals. This methodology strikes an optimal balance between numerical accuracy and computational efficiency, enabling precise statistical analysis without excessive resource demands. All simulations were conducted on a system equipped with an Intel(R) Core(TM) i7-7500U CPU (2.70–2.90 GHz), 12.0 GB RAM, and a 64-bit operating system, ensuring sufficient computational power for the tasks.

Example 1. To illustrate the performance of our numerical scheme, we consider the FTSSDE given by (1) in a one-dimensional spatial domain. The equation is parameterized as follows: the fractional derivative order is set to $\alpha = 0.95$, reflecting a near-integer temporal memory effect; the fractional Laplacian order is $\beta = 1.35$, which governs the spatial nonlocality; the diffusion coefficient is $\kappa_\beta = 0.01$, controlling the strength of diffusion; and the noise standard deviation is $\sigma = 0.3$, representing the intensity of stochastic forcing. The spatial domain is defined as $[c, c+L]$ with a length of L units, and the simulation runs over a total time of T_f. The FTSSDE is expressed as

$$ {}^{c}\partial_t^{\alpha} C(x,t) + \kappa_\beta(-\Delta)^{\beta/2} C(x,t) = \sigma W(x)\mathbb{B}_{\text{Bridge}}(t), \quad x \in [c, c+L],\, t \in [0, T_f], \tag{16} $$

where $W(x)$ denotes a spatial white noise process, and $\mathbb{B}_{\text{Bridge}}(t)$ represents a Brownian bridge process, introducing temporal stochasticity. The initial condition for the pollutant concentration $C(x,t)$ is specified as

$$ C(x,0) = C_0(x) = 5\text{sinc}(x), \quad x \in [c, c+L], \tag{17} $$

where the $\text{sinc}(x) = \frac{\sin(x)}{x}$ function provides a smooth, oscillatory profile shifted by 0.5 to ensure nonnegativity, mimicking a realistic initial distribution of a pollutant. The boundary conditions are as defined in (3), typically enforcing periodicity or zero-flux conditions to suit the physical context of the problem. This setup allows us to evaluate the numerical scheme's ability to capture the complex interplay between fractional derivatives, diffusion, and stochastic noise in a controlled yet challenging scenario.

Employing the sinc function as the initial condition provides a novel framework for studying pollutant dispersion dynamics. The $\text{sinc}(x) = \frac{\sin(x)}{x}$ function, characterized by a pronounced central peak and decaying oscillatory tails, serves as an effective model for capturing the spatial heterogeneity of pollutant concentrations, particularly in scenarios involving localized sources or

asymmetric distributions. This choice facilitates a detailed exploration of how pollutant sources interact with environmental factors and dispersion mechanisms, offering valuable insights into the complex behavior of environmental pollution. By leveraging the sinc function's unique properties, our approach enhances the ability to analyze the influence of fractional derivatives, stochastic noise, and diffusion processes, contributing to a deeper understanding of pollutant transport in diverse ecological settings.

In Example 1, Figure 3 illustrates the temporal evolution of the pollutant concentration $C(x,t)$ within a one-dimensional spatial domain $[-5,5]$, using the sinc function as the initial condition. The visualizations include three-dimensional surface plots and contour plots, generated through simulations employing both the Euler method and the KLE for Brownian noise. The domain, with a length of $L = 10$ units, is discretized into $N_x = 256$ spatial points to ensure high resolution in capturing spatial variations. The simulation spans a total time of $T_f = 1$ unit, divided into time steps of $\Delta t = 0.01$, providing fine temporal granularity for accurate tracking of the solution's evolution. For the KLE-based simulation, 512 terms are utilized to represent the stochastic noise, ensuring a robust approximation of the Brownian bridge process. These plots effectively demonstrate the numerical scheme's capability to model the intricate dynamics of pollutant dispersion under the influence of fractional operators and stochastic forcing, highlighting differences in the behavior of $C(x,t)$ between the Euler and KLE approaches.

Table 1: Convergence analysis for Euler and KLE simulations

	Euler Simulation		**KLE Simulation**	
Grid Size	**MSE**	**Convergence Order**	**MSE**	**Convergence Order**
512	0.1011	–	1.6259×10^{-4}	–
256	0.55561	2.4583	7.0254×10^{-3}	5.4333
128	3.6878	2.7306	0.11504	4.0335
64	8.3852	1.1851	0.34073	1.5665

Table 1 and Figure 4 present a comparative convergence analysis between KLE and Euler simulations for Brownian noise across uniform grid sizes from 64 to 512 points. The KLE simulation demonstrates markedly superior performance, achieving MSE values approximately three orders of magnitude lower than the Euler method at equivalent grid resolutions (e.g., 1.6×10^{-4} versus 0.1011 at 512 grid points). Moreover, the KLE approach exhibits exceptional convergence properties, with orders ranging from 1.5665 to 5.4333, substantially outperforming the Euler method's more modest convergence rates of 1.1851 to 2.7306. This remarkable difference in convergence behavior is clearly visualized in the log-log plots of Figure 4, where the steeper slope of the KLE simulation curve indicates its superior convergence rate.

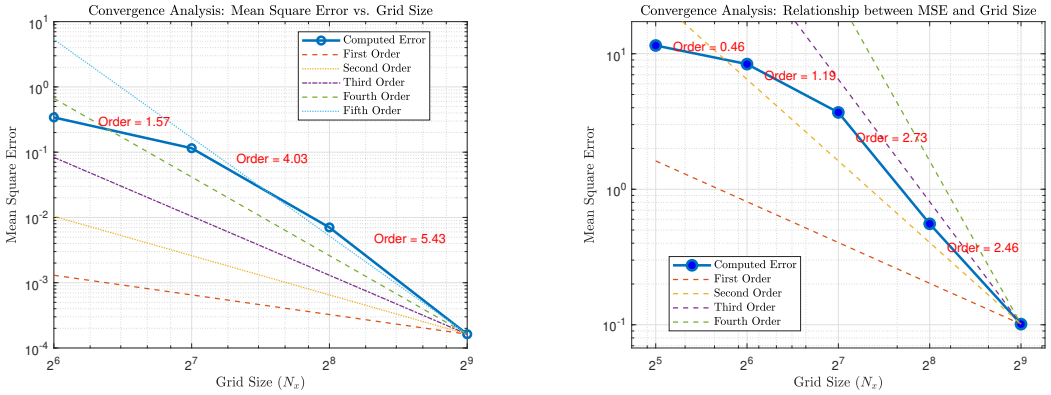

(a) Convergence analysis for KLE simulation

(b) Convergence analysis for Euler simulation

Figure 4: Convergence analysis showing the relationship between MSE and uniform grid resolution N_x. The analysis compares performance of the proposed method using both KLE and Euler approaches for Brownian noise simulation. Reference lines indicating different rates of convergence (ROCs) are included for comparison.

These findings have significant computational implications, as the KLE method can achieve comparable or superior accuracy with considerably coarser grids compared to the Euler approach. For instance, a KLE simulation with just 128 grid points ($MSE \approx 0.115$) delivers better accuracy than an Euler simulation with 512 points ($MSE \approx 0.101$), potentially yielding substantial computational savings. The superior performance of the KLE method can be attributed to its spectral decomposition approach, which effectively captures the essential stochastic features of Brownian motion, in contrast to the Euler method's incremental approximation strategy. This fundamental difference in methodology results in both enhanced accuracy and improved convergence properties, making the KLE approach particularly advantageous for applications requiring high precision numerical solutions of stochastic processes.

Example 2. To further validate the numerical scheme and explore the influence of different initial conditions on pollutant dispersion, we consider the FTSSDE given by (1) with a Gaussian initial distribution. The equation parameters remain consistent with Example 1: the fractional derivative order is $\alpha = 0.95$, the fractional Laplacian order is $\beta = 1.35$, the diffusion coefficient is $\kappa_\beta = 0.01$, and the noise standard deviation is $\sigma = 0.2$.

The initial condition for the pollutant concentration $C(x,t)$ is specified as a Gaussian distribution:

$$C(x,0) = C_0(x) = A \exp\left(-\frac{(x-x_0)^2}{2\sigma_{\text{gauss}}^2}\right) + C_{\text{medium}}, \quad x \in [c, c+L], \tag{18}$$

where $A = 5.0$ represents the peak concentration at the center of the distribution, $x_0 = 0$ is the center coordinate of the Gaussian profile, $\sigma_{\text{gauss}} = 1.5$ controls the spread of the initial

pollutant distribution, and $C_{\text{medium}} = 0.01$ denotes the background concentration level in the medium. This Gaussian profile models a realistic scenario where pollutants are initially concentrated around a point source with smooth decay away from the center, commonly observed in environmental contamination from localized industrial discharge or chemical spills.

The Gaussian initial condition provides an ideal test case for evaluating the numerical scheme's performance in handling smooth, bell-shaped distributions that are prevalent in environmental modeling. Unlike the oscillatory nature of the sinc function used in Example 1, the Gaussian profile offers a monotonic decay from the central peak, allowing for a clearer observation of how fractional derivatives and stochastic noise influence the spreading and evolution of pollutant plumes over time. The boundary conditions follow (3), maintaining consistency with the periodic domain setup employed throughout this study.

In Example 2, Figure 5 presents the temporal evolution of the pollutant concentration $C(x,t)$ within the same one-dimensional spatial domain $[-5,5]$ as in Example 1, but using the Gaussian distribution as the initial condition. The domain maintains a length of $L = 10$ units, discretized into $N_x = 256$ spatial points, with the simulation spanning a total time of $T_f = 1$ unit using time steps of $\Delta t = 0.01$. The visualizations include both three-dimensional surface plots and contour plots, comparing simulations employing the Euler method and the KLE for Brownian noise representation. For the KLE-based simulation, 512 terms are utilized to ensure robust approximation of the stochastic processes. These plots demonstrate the smooth evolution of the initially concentrated Gaussian pollutant plume as it disperses under the combined influence of fractional diffusion and stochastic forcing, clearly illustrating the differences in numerical behavior between the two simulation approaches.

Table 2: Convergence analysis for Euler and KLE simulations - Example 2

	Euler Simulation		**KLE Simulation**	
Grid Size	**MSE**	**Convergence Order**	**MSE**	**Convergence Order**
512	0.067526	–	1.0922×10^{-4}	–
256	0.41985	2.6364	6.9163×10^{-3}	5.9847
128	3.2346	2.9457	0.11481	4.0531
64	8.1412	1.3316	0.34036	1.5678

Table 2 and Figure 6 present a comprehensive convergence analysis for the Gaussian initial condition case, comparing KLE and Euler simulations across uniform grid sizes ranging from 64 to 512 points. Consistent with the findings from Example 1, the KLE simulation demonstrates markedly superior performance, achieving MSE values approximately three orders of magnitude lower than the Euler method at equivalent grid resolutions. For instance, at 512 grid points, the

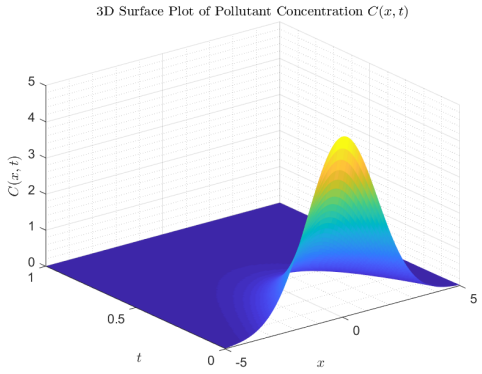

(a) Three-dimensional surface plot of pollutant concentration $C(x,t)$ using Euler Brownian noise simulation.

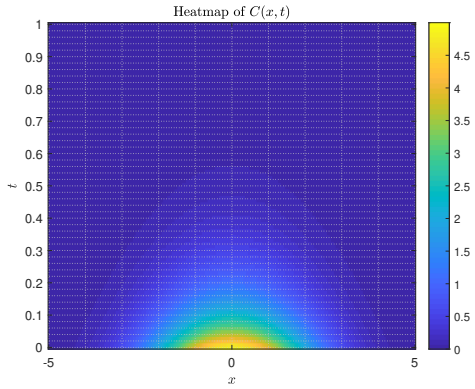

(b) Contour plot of pollutant concentration $C(x,t)$ with Euler simulation of Brownian noise.

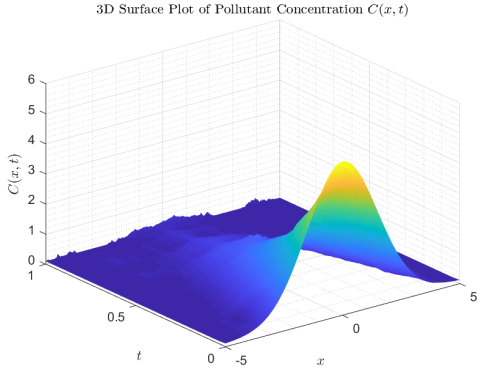

(c) Three-dimensional surface plot of pollutant concentration $C(x,t)$ using KLE Brownian noise simulation.

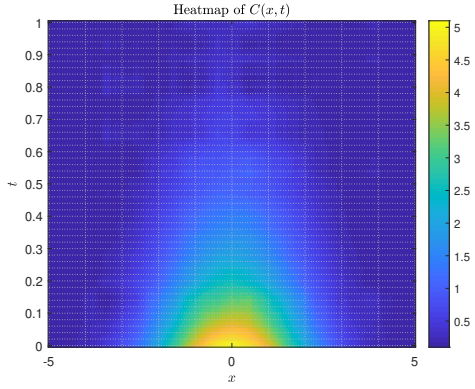

(d) Contour plot of pollutant concentration $C(x,t)$ with KLE Brownian noise simulation.

Figure 5: Example 2: Three-dimensional surface representations and contour plots displaying pollutant concentration $C(x,t)$ over space and time, using the Gaussian distribution as the initial condition.

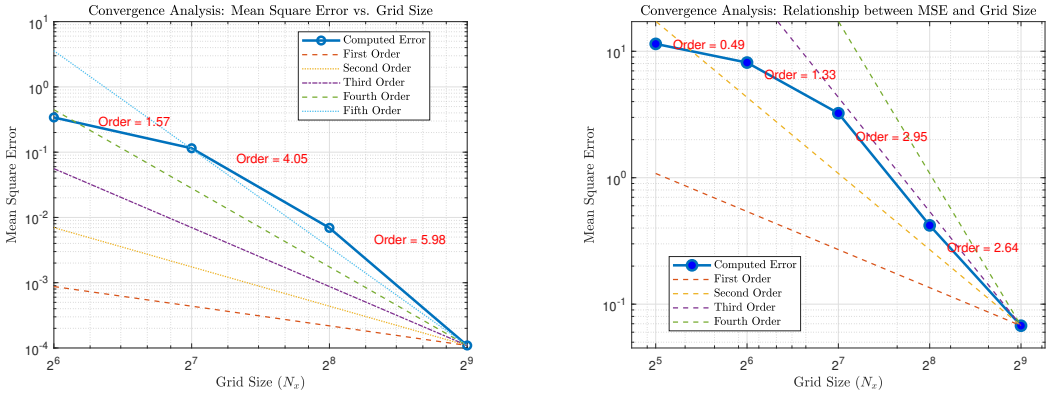

(a) Convergence analysis for KLE simulation

(b) Convergence analysis for Euler simulation

Figure 6: Example 2: Convergence analysis showing the relationship between MSE and uniform grid resolution N_x for the Gaussian initial condition. The analysis compares performance of the proposed method using both KLE and Euler approaches for Brownian noise simulation. Reference lines indicating different rates of convergence (ROCs) are included for comparison.

KLE method achieves an MSE of 1.0922×10^{-4} compared to the Euler method's MSE of 0.067526. The KLE approach also exhibits exceptional convergence properties, with convergence orders ranging from 1.5678 to 5.9847, substantially outperforming the Euler method's convergence rates of 1.3316 to 2.9457.

The Gaussian initial condition results reinforce the computational advantages of the KLE methodology observed in the sinc function case. The smooth, bell-shaped profile of the Gaussian distribution allows for even more pronounced differences in convergence behavior between the two methods, as evidenced by the steeper slope in the KLE convergence curve shown in Figure 6. Notably, the KLE method with the Gaussian initial condition achieves the highest convergence order observed in this study (5.9847 between 512 and 256 grid points), demonstrating the method's particular effectiveness with smooth initial conditions.

This consistency across different initial conditions validates the robustness of the KLE approach and its suitability for a wide range of environmental modeling applications involving pollutant dispersion. The superior convergence properties of the KLE method make it especially attractive for computational scenarios where high accuracy is required while maintaining reasonable computational costs, as a KLE simulation with 128 grid points (MSE ≈ 0.115) delivers significantly better accuracy than an Euler simulation with 512 points (MSE ≈ 0.068).

6 Conclusion

This study successfully investigated a FTSSDE for modeling pollutant concentration, integrating Caputo fractional derivatives, fractional Laplacians, and stochastic noise through Brownian motion and Brownian bridges. By employing the KLE for noise simulation, FFT for spatial discretization, and the L1-algorithm for temporal fractional derivatives, we demonstrated the superior performance of advanced numerical methods over traditional approaches. Two comprehensive numerical examples—one using sinc function initial conditions to handle oscillatory spatial distributions and another employing Gaussian initial conditions for smooth concentration profiles—consistently validated the exceptional accuracy and efficiency of the KLE method. The approach achieved MSEs approximately three orders of magnitude lower than traditional Euler methods while requiring significantly fewer computational resources, with simulations using fewer grid points consistently delivering better accuracy than conventional methods with higher resolution grids.

The numerical results revealed the critical influence of fractional parameters in capturing anomalous diffusion behaviors, providing deeper insights into pollutant dynamics in complex environmental systems compared to classical diffusion models. The demonstrated computational advantages and robust performance across diverse initial conditions made this fractional stochastic approach particularly valuable for large-scale environmental applications, including groundwater contamination, atmospheric dispersion, and ecological impact assessments. These findings underscore the significant potential for practical implementation in environmental risk assessment and remediation planning, while future research opportunities include adaptive numerical schemes, multi-dimensional extensions, coupled transport-reaction systems, and integration with real-world environmental data to further enhance model predictions and broaden their utility in environmental science applications.

Acknowledgments

The authors extend their gratitude to the anonymous referees and editor for their thoughtful reviews and recommendations.

Funding

This research received no external funding.

Conflicts of Interest

All authors jointly worked on the results and they read and approved the final manuscript, and also declare that they have no competing interests.

References

[1] Adebisi, A.F., Gbolagade, G.M., Ogunniran, M.O. and Ajewole, K.P. *Convergence and stability analysis of finite difference methods, Caputo derivatives, and collocation methods applied to space fractional diffusion equations*, Proc. Int. Conf. on Science, Engineering and Business for Driving Sustainable Development Goals (SEB4SDG 2024), 2024.

[2] Adel, M. *Numerical simulations for the variable order two-dimensional reaction sub-diffusion equation: linear and nonlinear*, Fractals, 2022.

[3] Baeumer, B., Kovács, M. and Meerschaert, M.M. *Numerical solutions for fractional reaction-diffusion equations*, Comput. Math. Appl., 55 (10) (2008), 2212–2226.

[4] Cho, H., Venturi, D. and Karniadakis, G.E. *Karhunen-Loève expansion for multi-correlated stochastic processes*, Probabilist. Eng. Mech., 34 (2013), 157–167.

[5] Chow, W.C. *Brownian bridge*, Wiley Interdiscip. Rev.: Comput. Stat., 1 (3) (2009), 362–367.

[6] Dos Santos, M.A.F. *Fractional Prabhakar derivative in diffusion equation with non-static stochastic resetting*, Physics (Switzerland), 1 (2) (2019), 288–302.

[7] Goulart, A.G.O., Lazo, M.J., Suarez, J.M.S. and Moreira, D.M. *Fractional derivative models for atmospheric dispersion of pollutants*, Physica A, 477 (2017), 9–19.

[8] Guo, B., Pu, X. and Huang, F. *Fractional partial differential equations and their numerical solutions*, World Scientific, Singapore, 2015.

[9] Hamrouni, W. and Abdennadher, A. *Random walk's models for fractional diffusion equation*, Discrete Contin. Dyn. Syst. Ser. B, 21(10) (2016), 3339–3356.

[10] Hernandez-Martinez, E., Valdés-Parada, F., Alvarez-Ramirez, J. and Morales-Zarate, E. *A Green's function approach for the numerical solution of a class of fractional reaction-diffusion equations*, Math. Comput. Simul., 120 (2016), 36–52.

[11] Ju, Y., Yang, J., Liu, Z. and Xu, Q. *Meshfree methods for the variable-order fractional advection-diffusion equation*, Math. Comput. Simul., 217 (2023), 287–300.

[12] Kim, M., Mert Coskun, O., Ordu, S. and Mutlu, R. *Modeling pollutant diffusion in the ground using conformable fractional derivative in spherical coordinates with complete symmetry*, Symmetry, 16 (2024), 427.

[13] Kundu, A., Bernardin, C., Saito, K. and Dhar, A. *Fractional equation description of an open anomalous heat conduction set-up*, J. Stat. Mech. Theory Exp., 2019(1) (2019), 013203.

[14] Lord, G.J., Powell, C.E. and Shardlow, T. *An introduction to computational stochastic PDEs*, Cambridge University Press, 2014.

[15] Mohammed, W.W., Alshammari, M., Cesarano, C. and El-Morshedy, M. *Brownian motion effects on the stabilization of stochastic solutions to fractional diffusion equations with polynomials*, Mathematics, 10 (3) (2022), 359.

[16] Moghaddam, B.P., Zaky, M.A., Lopes, A.M. and Galhano, A. *A Fractional time-space stochastic advection-diffusion equation for modeling atmospheric moisture transport at ocean-atmosphere interfaces*, Fractal Fract., 8 (2024), 163.

[17] Moghaddam, B.P., Babaei, A., Dabiri, A. and Galhano, A. *Fractional stochastic partial differential equations: Numerical advances and practical applications—A state of the art review*, Symmetry, 16 (2024), 257.

[18] Moniri, Z., Babaei, A. and Moghaddam, B.P. *Robust numerical framework for simulating 2D fractional time–space stochastic diffusion equation driven by spatio-temporal noise: L1-FFT hybrid approach*, Commun. Nonlinear Sci. Numer. Simul., 136 (2025), 109612.

[19] Noor, S., Alrowaily, A.W., Alqudah, M. and El-Tantawy, S.A. *Innovative solutions to the fractional diffusion equation using the Elzaki transform*, Math. Comput. Appl., 29 (1) (2024), 7.

[20] Poirion, F. and Zentner, I. *Non-Gaussian non-stationary models for natural hazard modeling*, Appl. Math. Model., 37 (1-2) (2013), 533–546.

[21] Poirion, F. and Zentner, I. *Stochastic model construction of natural hazards given experimental measures*, Proc. 11th Int. Conf. on Structural Safety and Reliability (ICOSSAR), 2013.

[22] Qu, B., Addison, P.S. and Dong, Y. *Fractal simulation of diffusion of pollutants in open ocean*, Adv. Sci. Technol. Water Resour., 36 (2016), 10–22.

[23] Rakhimov, A. and Ahmedov, A. *On the fundamental solution of the Cauchy problem for time fractional diffusion equation on the sphere*, Malays. J. Math. Sci., 6 (2) (2012), 215–226.

[24] Rashidinia, J., Molavi-Arabshahi, M. and Yousefi, M. *An efficient approach for solving a class of fractional anomalous diffusion equation with convergence*, Phys. Scr., 99 (2024), 105203.

[25] Ray, S.S., Chaudhuri, K.S. and Bera, R.K. *Application of modified decomposition method for the analytical solution of space fractional diffusion equation*, Appl. Math. Comput., 197(2) (2008), 667–673.

[26] Ray, S.S. *Analytical solution for the space fractional diffusion equation by two-step Adomian Decomposition Method*, Commun. Nonlinear Sci. Numer. Simul., 14(3) (2009), 1295–1306.

[27] Singh, A.K. and Mehra, M. *Difference methods for stochastic space fractional diffusion equation driven by additive space–time white noise via Wong–Zakai approximation*, J. Math. Chem., 61 (2023), 2263–2283.

[28] Sultana, S. *Analysis of a generalized proportional fractional stochastic differential equation incorporating Carathéodory's approximation and applications*, Open Phys., 22 (2024), 20240155.

[29] Sylvain, T.T.A., Patrice, E.L.E.A., Marie, E.E.J. and Hubert, B.-B.G. *A unified three-dimensional extended fractional analytical solution for air pollutants dispersion*, Fractals, 30 (7) (2022), 2250180.

[30] Yuan, X., Yu, Y. and Ren, G. *Random attractors for fractional stochastic reaction–diffusion systems with fractional Brownian motion*, Chaos Solitons Fractals, 183 (2025), 114579.

[31] Zhang, Y., Zhou, D., Wei, W. and Chen, X. *Hierarchical fractional advection-dispersion equation (FADE) to quantify anomalous transport in river corridor over a broad spectrum of scales: Theory and applications*, Mathematics, 9 (6) (2021), 639.